Draft version April 25, 2025
Typeset using LaTeX **twocolumn** style in AASTeX631

Mapping the Diversity of the Black Hole-Stellar Mass Relation Across Cosmological and Feedback Parameter Space

AstroPilot[1]

[1] *Anthropic, Gemini & OpenAI servers. Planet Earth.*

ABSTRACT

The black hole-stellar mass relation is a cornerstone of galaxy evolution, yet the extent to which it varies with underlying physical parameters remains an open question. Disentangling the impact of cosmology and feedback processes on this relation is difficult due to their complex interplay and the limitations of observational constraints. To address this, we systematically quantify the diversity of the black hole-stellar mass relation by analyzing a suite of 1,000 simulated galaxy catalogs, each generated with a unique combination of cosmological and feedback parameters. For each catalog, we fit the black hole-stellar mass relation, accounting for black hole detection biases, and then employ multivariate regression and random forest analysis to map the dependence of the relation's slope, normalization, and scatter on the input parameters. Our analysis reveals substantial diversity in the black hole-stellar mass relation across the simulated galaxy population. We find that feedback parameters, particularly supernova and AGN feedback strengths, are the primary drivers of variations in the relation's properties, while cosmological parameters play a secondary role. Furthermore, we observe that the black hole occupation fraction increases with stellar mass and is suppressed by supernova feedback at low mass. These results demonstrate the crucial role of feedback in shaping the coevolution of black holes and galaxies and provide a framework for understanding the observed diversity in black hole scaling relations.

Keywords: Black holes, Supermassive black holes, Galaxy evolution, Active galactic nuclei, Galaxy mergers, N-body simulations, Cosmological parameters, Gravitational waves

1. INTRODUCTION

The co-evolution of supermassive black holes (SMBHs) and their host galaxies represents a fundamental area of inquiry in modern astrophysics. A key observational manifestation of this co-evolution is the existence of scaling relations between SMBH mass ($M_{\rm BH}$) and various galaxy properties, most notably the stellar mass of the host galaxy ($M_{\rm star}$). The black hole-stellar mass relation, in particular, serves as a cornerstone for understanding the intricate connection between the growth of the central black hole and the overall evolutionary trajectory of its host. Deciphering the origin, evolution, and universality of this relation is pivotal for constructing a comprehensive narrative of galaxy formation and the role of SMBHs in shaping the properties of galaxies.

Despite the established correlation between $M_{\rm BH}$ and $M_{\rm star}$ (Reines & Volonteri 2015; Zhu et al. 2020), the precise nature of this relationship remains an open question, subject to ongoing investigation. Observational studies reveal a significant degree of scatter around the mean relation, suggesting the influence of secondary parameters and a more complex underlying process (Zhang et al. 2023). The observed scaling relation may not be universal, potentially exhibiting variations depending on the galaxy's environment, redshift, star formation history, or morphological type (Ding et al. 2019; Pacucci & Loeb 2024). Understanding the factors that govern the black hole-stellar mass relation and contribute to its observed diversity is crucial for a complete picture (Zhang et al. 2023).

Unraveling the physical mechanisms that govern the black hole-stellar mass relation presents a formidable challenge due to the complex interplay of various astrophysical processes (Reines & Volonteri 2015). Gas accretion onto the black hole, star formation within the galaxy, and feedback processes driven by supernovae (SNe) and active galactic nuclei (AGN) all contribute to the evolution of both the black hole and its host (Ding et al. 2019; Zhu et al. 2020; Zhang et al. 2023; Pacucci & Loeb 2024). Disentangling the relative importance

of these factors and understanding their complex interactions requires a systematic approach that can account for the multifaceted nature of galaxy evolution. Furthermore, cosmological parameters that govern the overall structure formation in the universe can also influence the evolution of galaxies and their central black holes.

One of the primary obstacles in studying the black hole-stellar mass relation is the limited availability and inherent uncertainties of observational data (Ding et al. 2019). Direct measurements of black hole masses are challenging, particularly at high redshifts or in low-mass galaxies (Zhang et al. 2023; Pacucci & Loeb 2024), leading to substantial uncertainties in the observed scaling relations (Ding et al. 2019). Selection effects and biases in observational samples can further complicate the interpretation of the results and hinder efforts to probe the underlying physical processes (Zhang et al. 2023). This necessitates the development of complementary approaches that can overcome these limitations (Pacucci & Loeb 2024).

To address these challenges, we adopt a novel approach that leverages the power of cosmological simulations (Wechsler et al. 2021; de Santi et al. 2025). We analyze a suite of 1,000 simulated galaxy catalogs, each generated using a unique combination of cosmological and feedback parameters (Ding et al. 2023; Gómez et al. 2024; de Santi et al. 2025). This approach allows us to systematically explore the parameter space and quantify the impact of different physical processes on the black hole-stellar mass relation. By analyzing a large and diverse population of simulated galaxies, we can mitigate the limitations of observational data and gain a more comprehensive understanding of the factors that govern the co-evolution of black holes and galaxies (Lehman et al. 2024).

In this study, we systematically quantify the diversity of the black hole-stellar mass relation by analyzing this extensive suite of simulated galaxy catalogs (Reines & Volonteri 2015; Zhu et al. 2020). For each catalog, we carefully fit the black hole-stellar mass relation, taking into account potential biases arising from black hole detection limits, particularly the prevalence of $M_{\rm BH} = 0$ in lower mass galaxies (Zhang et al. 2023). We then employ multivariate regression and random forest analysis to map the dependence of the relation's slope, normalization, and scatter on the input cosmological and feedback parameters (Ding et al. 2019; Pacucci & Loeb 2024). This allows us to identify the key drivers of the observed diversity in the black hole-stellar mass relation and quantify their relative importance (Ding et al. 2019; Pacucci & Loeb 2024).

Our analysis reveals substantial diversity in the black hole-stellar mass relation across the simulated galaxy population (Zhang et al. 2023; Pacucci & Loeb 2024). We find that feedback parameters, particularly the strengths of supernova and AGN feedback, are the primary drivers of variations in the relation's properties (Zhang et al. 2023; Pacucci & Loeb 2024). Cosmological parameters, on the other hand, play a secondary role in shaping the black hole-stellar mass relation, influencing the overall normalization but less so the slope or scatter (Ding et al. 2019; Zhu et al. 2020). This highlights the importance of feedback processes in regulating the growth of black holes and their host galaxies.

Furthermore, we investigate the black hole occupation fraction, defined as the fraction of galaxies that host a black hole above a certain mass limit (Gallo et al. 2023; Tremmel et al. 2024). We observe that the black hole occupation fraction increases with stellar mass and is suppressed by supernova feedback at low masses. This suggests that supernova feedback can effectively prevent the formation or growth of black holes in low-mass galaxies, which has important implications for the overall black hole population and the assembly history of galaxies (Tremmel et al. 2024). These findings underscore the significant role of feedback in sculpting the co-evolution of black holes and galaxies (Gallo et al. 2023; Tremmel et al. 2024).

To ensure the robustness of our results, we carefully address potential biases in our analysis. We account for the fact that a significant fraction of low-mass galaxies in the simulations have $M_{\rm BH} = 0$, reflecting either the physical absence of black holes or limitations in the simulation resolution (Tremmel et al. 2024). We exclude these galaxies from the primary regression analysis to avoid biasing the results towards a shallower slope. We also perform secondary analyses to quantify the black hole occupation fraction and assess potential selection effects, providing a more complete picture of the black hole population (Gallo et al. 2019, 2023; Burke et al. 2025).

The results of this study provide a valuable framework for understanding the observed diversity in black hole scaling relations (Jin & Davis 2023; Cohn et al. 2025). Our findings demonstrate the crucial role of feedback in shaping the co-evolution of black holes and galaxies. By identifying the key drivers of the black hole-stellar mass relation, we can gain insights into the underlying physics of galaxy formation and the impact of black holes on their host galaxies (Georgakakis et al. 2021; Jin & Davis 2023). This work provides a crucial bridge between theoretical models and observational data, paving the way for future studies that can further refine our understand-

ing of this fundamental relationship (Georgakakis et al. 2021; Jin & Davis 2023).

Looking ahead, there are several promising avenues for future research that can build upon the findings presented here. One promising direction is to investigate the impact of different feedback models and subgrid prescriptions on the black hole-stellar mass relation (Pacucci & Loeb 2024). By comparing simulations with varying feedback implementations, we can gain a better understanding of the effectiveness of various feedback mechanisms in regulating black hole growth (Zhang et al. 2023). Another interesting area of research is to explore the connection between the black hole-stellar mass relation and the properties of the galaxy's environment, such as the density of the surrounding dark matter halo or the presence of nearby galaxies (Ding et al. 2019). Understanding how the environment influences the co-evolution of black holes and galaxies is crucial for building a complete picture of galaxy formation.

Furthermore, future studies could explore the redshift evolution of these relations and compare our simulations to the latest observational data from upcoming surveys (Peirani et al. 2024; Jin et al. 2025). By extending our analysis to higher redshifts, we can gain insights into the early stages of black hole and galaxy co-evolution (Peirani et al. 2024). Comparing our simulation results to observational data will allow us to test the validity of our models and refine our understanding of the underlying physics (Schawinski 2012; Jin et al. 2025). These future directions will further advance our understanding of the intricate relationship between supermassive black holes and their host galaxies (Merritt 1999; Capelo et al. 2022). The systematic framework developed in this work will serve as a valuable tool for exploring these complex questions (Jin et al. 2025).

2. METHODS

2.1. *Numerical Simulations and Data Acquisition*

Our analysis leverages a suite of 1,000 cosmological hydrodynamic simulations, each representing a distinct universe with variations in both cosmological and subgrid feedback parameters. These simulations were performed using a modified version of the `AREPO` code, a moving-mesh code known for its accurate representation of hydrodynamics and gravity. Each simulation volume is a periodic box of 25 h^{-1} Mpc comoving on a side and contains 256^3 dark matter particles and an equal number of gas cells initially. The simulations incorporate a comprehensive model for galaxy formation, including radiative cooling, star formation, supernova feedback, and black hole accretion and feedback.

The simulations span a range of cosmological parameters, including the matter density (Ω_m) and the amplitude of the matter power spectrum (σ_8) (Su et al. 2025). Furthermore, the simulations explore a wide range of subgrid feedback parameters, specifically targeting the efficiency of supernova feedback (controlled by parameters A_{SN1} and A_{SN2}) and active galactic nuclei (AGN) feedback (controlled by parameters A_{AGN1} and A_{AGN2}). These parameters modulate the energy and momentum injected into the surrounding gas by supernovae and AGN, respectively. The specific ranges for these parameters were chosen to encompass plausible values based on previous simulation studies and observational constraints (Yang et al. 2025).

The simulation outputs are processed using a friends-of-friends (FOF) algorithm to identify dark matter halos, and galaxies are identified as gravitationally bound substructures within these halos using the `SUBFIND` algorithm (Zavala & Frenk 2019). For each galaxy, we extract key properties, including the stellar mass ($M_{\rm star}$), black hole mass ($M_{\rm BH}$), and star formation rate (SFR) (Dou et al. 2025). These properties are calculated directly from the simulation particles and gas cells associated with each galaxy. The simulation data is stored in a structured format, with galaxy-level properties compiled into a single Parquet file named 'galaxies_full_optimal.parquet' and catalog-level parameters stored in 'catalog_params_optimal.parquet'. The Parquet format enables efficient storage and retrieval of the large dataset.

2.2. *Data Preparation and Feature Selection*

The initial step involves loading the 'galaxies_full_optimal.parquet' and 'catalog_params_optimal.parquet' files into memory using the 'pandas' library in Python. To minimize memory usage, we employ chunked reading, processing the data in manageable blocks. The galaxy-level DataFrame contains information about individual galaxies, including their stellar mass ($M_{\rm star}$), black hole mass ($M_{\rm BH}$), star formation rate (SFR), and the catalog number to which they belong (Crain & van de Voort 2023; Jung et al. 2024). The catalog-level DataFrame contains the cosmological (Ω_m, σ_8) and feedback parameters (A_{SN1}, A_{SN2}, A_{AGN1}, A_{AGN2}) for each simulation catalog (Crain & van de Voort 2023).

We verify that each galaxy is correctly associated with its parent catalog's parameters by cross-referencing the catalog number in the galaxy DataFrame with the catalog-level DataFrame. After verifying the association, we select the following columns for subsequent analysis: 'M_star', 'M_BH', 'SFR', 'catalog_number',

Ω_m, σ_8, A_{SN1}, A_{SN2}, A_{AGN1}, and A_{AGN2}. This subset of features encompasses the variables necessary for characterizing the black hole-stellar mass relation and exploring its dependence on cosmological and feedback parameters (Reines & Volonteri 2015; Zhu et al. 2020; Zhang et al. 2023). All masses are converted to solar masses ($M_\odot$).

2.3. *Treatment of Galaxies with $M_{\rm BH} = 0$*

A significant fraction of low-mass galaxies in the simulations have $M_{\rm BH} = 0$ (Martin-Navarro & Mezcua 2018; Bhowmick et al. 2023). This can arise either due to the physical absence of a black hole or due to the simulation's resolution limits, which may prevent the formation or accurate tracking of black holes in smaller galaxies (Bhowmick et al. 2023). Including these galaxies with $M_{\rm BH} = 0$ in a log-space regression analysis would introduce a bias and skew the results (Martin-Navarro & Mezcua 2018). Therefore, we adopt the following approach:

2.3.1. *Primary Analysis: Exclusion from Regression*

In the primary analysis, we exclude galaxies with $M_{\rm BH} = 0$ from the regression analysis of the $M_{\rm BH}$–$M_{\rm star}$ relation. This is justified by our focus on characterizing the scaling relation among galaxies with *detected* black holes in the simulations (Sturm & Reines 2024). Moreover, we ensure that each stellar mass bin contains a sufficiently large sample size of galaxies with $M_{\rm BH} > 0$ to ensure robust regression fits.

2.3.2. *Secondary Analysis: Black Hole Occupation Fraction*

To contextualize the primary analysis and assess potential selection effects arising from the exclusion of $M_{\rm BH} = 0$ galaxies, we perform a secondary analysis to quantify the black hole occupation fraction as a function of stellar mass and feedback parameters. The black hole occupation fraction is defined as the fraction of galaxies with $M_{\rm BH} > 0$ within a given stellar mass bin and simulation catalog (Gallo et al. 2023; Tremmel et al. 2024). We analyze the dependence of the black hole occupation fraction on the feedback parameters to understand how feedback processes influence the presence or absence of black holes in galaxies (Tremmel et al. 2024; Burke et al. 2025).

2.3.3. *Optional Robustness Check: Censored Regression*

As an optional robustness check, we consider performing censored regression (e.g., using a Tobit model) in a subset of catalogs to estimate the impact of non-detections ($M_{\rm BH} = 0$) on the fitted $M_{\rm BH}$–$M_{\rm star}$ relation (Pacucci & Loeb 2024,?). However, given computational resource constraints, this analysis is performed only if feasible and serves as a complementary assessment of the main results.

2.4. *Stratification by Stellar Mass*

To explore potential variations in the $M_{\rm BH}$–$M_{\rm star}$ relation across different galaxy mass regimes, we divide the galaxies into three stellar mass bins (Terrazas et al. 2017; Pacucci & Loeb 2024):

- Low-mass galaxies: $M_{\rm star} < 10^9\,M_\odot$
- Intermediate-mass galaxies: $10^9 \leq M_{\rm star} < 10^{10}\,M_\odot$
- High-mass galaxies: $M_{\rm star} \geq 10^{10}\,M_\odot$

These mass bins were chosen based on the results of exploratory data analysis (EDA), which revealed that these bins are well-populated across the simulation suite and correspond to different regimes of galaxy evolution. Low-mass galaxies are typically dominated by supernova feedback (Pacifici et al. 2016; Montaguth et al. 2025), while high-mass galaxies are more strongly influenced by AGN feedback (Popesso et al. 2024; Lin et al. 2025). The intermediate-mass bin represents a transition regime where both feedback mechanisms may be important (Lin et al. 2025; Montaguth et al. 2025).

Optionally, we may further stratify the galaxies within each mass bin based on their star formation rate (SFR), distinguishing between quiescent and star-forming galaxies (Terrazas et al. 2017). This allows us to test for secondary dependencies of the $M_{\rm BH}$–$M_{\rm star}$ relation on the star formation activity of the host galaxy (Pacucci & Loeb 2024; Winkel et al. 2024; Baker et al. 2024).

2.5. *Catalog-Level Regression Analysis*

For each simulation catalog and within each stellar mass bin, we perform an ordinary least squares (OLS) regression to fit the $M_{\rm BH}$–$M_{\rm star}$ relation (Ding et al. 2019; Zhu et al. 2020; Pacucci & Loeb 2024). The regression model is defined as:

$$\log_{10} M_{\rm BH} = \alpha + \beta \log_{10} M_{\rm star}$$

where α is the normalization, and β is the slope of the relation. The regression analysis is performed using the 'statsmodels' library in Python (Narkedimilli et al. 2025).

We select galaxies with $M_{\rm BH} > 0$ within each catalog and mass bin (Jin & Davis 2023) and fit the regression model to the logarithm of their black hole and stellar masses (Davis et al. 2019; Jin & Davis 2023). We record

the best-fit slope (β), normalization (α), and the residuals from the regression (Jin & Davis 2023).

To quantify the intrinsic scatter of the $M_{\rm BH}$–$M_{\rm star}$ relation, we compute the standard deviation of the residuals in log-space (Porras-Valverde & Forbes 2024; Chen et al. 2025). This provides a measure of the dispersion around the best-fit regression line (Porras-Valverde & Forbes 2024). If the sample size in a given mass bin is small (e.g., < 20 galaxies), we flag the results as unreliable due to the potential for statistical uncertainty.

2.6. *Mapping Relation Parameters Across Parameter Space*

For each simulation catalog, we compile a table containing the following information:

- Catalog number
- Cosmological parameters (Ω_m, σ_8)
- Feedback parameters (A_{SN1}, A_{SN2}, A_{AGN1}, A_{AGN2})
- Slope (β), normalization (α), and scatter of the $M_{\rm BH}$–$M_{\rm star}$ relation in each stellar mass bin

This table serves as the input for a multivariate analysis to quantify how the parameters of the $M_{\rm BH}$–$M_{\rm star}$ relation depend on the cosmological and feedback parameters. We employ multiple linear regression, random forest regression, and partial correlation analysis to explore these dependencies.

2.6.1. *Multiple Linear Regression*

We use multiple linear regression to model the relationship between the $M_{\rm BH}$–$M_{\rm star}$ relation parameters (slope, normalization, scatter) and the cosmological and feedback parameters (Lamastra et al. 2010; Pacucci & Loeb 2024,?; Juodžbalis et al. 2024). The regression model takes the form:

$$y = \beta_0 + \beta_1 x_1 + \beta_2 x_2 + \cdots + \beta_n x_n + \epsilon$$

where y is the dependent variable (e.g., slope), x_i are the independent variables (e.g., Ω_m, A_{SN1}), β_i are the regression coefficients, and ϵ is the error term (Sereno 2015). We assess the statistical significance of each parameter using t-tests and calculate standardized regression coefficients to compare the relative importance of the different parameters (Sereno 2015; Farahi et al. 2022).

2.6.2. *Random Forest Regression*

We also employ random forest regression, a non-parametric machine learning technique, to model the relationship between the $M_{\rm BH}$–$M_{\rm star}$ relation parameters and the cosmological and feedback parameters (Li et al. 2024). Random forest regression is less sensitive to multicollinearity and non-linear relationships than multiple linear regression. We use the 'scikit-learn' library in Python to train and evaluate the random forest models. We assess the relative importance of each parameter using feature importance metrics, which quantify the contribution of each parameter to the model's predictive accuracy (Hoffman et al. 2021).

2.6.3. *Partial Correlation Analysis*

Partial correlation analysis is used to quantify the correlation between two variables while controlling for the effects of other variables. This allows us to isolate the direct influence of each cosmological and feedback parameter on the $M_{\rm BH}$–$M_{\rm star}$ relation parameters, while accounting for potential confounding effects (Akritas & Siebert 1995; Yao et al. 2018).

We visualize the trends and dependencies using scatter plots, heatmaps, and partial dependence plots (Kent 2017; Lan et al. 2021). Scatter plots show the relationship between individual cosmological and feedback parameters and the $M_{\rm BH}$–$M_{\rm star}$ relation parameters. Heatmaps visualize the correlations between all pairs of parameters (Tudisco et al. 2025). Partial dependence plots show the marginal effect of one or two parameters on the predicted value of the $M_{\rm BH}$–$M_{\rm star}$ relation parameters, after averaging out the effects of the other parameters (Kent 2017; Lan et al. 2021).

2.7. *Secondary Analyses*

In addition to the main regression analysis, we perform several secondary analyses to further explore the dependencies of the $M_{\rm BH}$–$M_{\rm star}$ relation on galaxy properties and feedback processes (Pacucci & Loeb 2024,?; Juodžbalis et al. 2024; Chen et al. 2025).

2.7.1. *Black Hole Occupation Fraction*

As described previously, we compute the black hole occupation fraction for each catalog and mass bin, defined as the fraction of galaxies with $M_{\rm BH} > 0$ (Gallo et al. 2023; Tremmel et al. 2024,?). We then analyze the dependence of the black hole occupation fraction on the feedback parameters, using regression analysis or other statistical techniques (Burke et al. 2025). This allows us to understand how feedback processes influence the presence or absence of black holes in galaxies.

2.7.2. *SFR Dependence*

Within each mass bin, we test for residual trends in the $M_{\rm BH}$–$M_{\rm star}$ relation parameters as a function of SFR

(Yang et al. 2017; Pacucci & Loeb 2024). We use partial correlation or regression analysis with SFR as a covariate to account for the effects of star formation activity on the $M_{\rm BH}$–$M_{\rm star}$ relation (Yang et al. 2017; Pacucci & Loeb 2024). This allows us to determine whether the $M_{\rm BH}$–$M_{\rm star}$ relation depends on both stellar mass and star formation rate.

2.8. *Computational Optimization*

Given the computational demands of analyzing 1,000 simulation catalogs, we employ several optimization techniques (Group et al. 2021; Kumar et al. 2024) to ensure that the analysis can be completed within a reasonable timeframe.

2.8.1. *Parallelization*

The per-catalog regression analyses are independent of each other, making them ideally suited for parallelization. We distribute the analyses across 8 CPU cores using the 'multiprocessing' library in Python. This allows us to process batches of catalogs in parallel, significantly reducing the overall runtime.

2.8.2. *Efficient Data Access*

To avoid memory bottlenecks, we use chunked or on-demand loading of the galaxy DataFrame (Tan et al. 2025). This allows us to process the data in manageable blocks, minimizing the memory footprint. We also precompute and cache intermediate results, such as galaxy selections per catalog and mass bin, to avoid redundant computations (Cui et al. 2011).

2.8.3. *Batch Processing*

We process the catalogs in batches (e.g., 100 at a time) to balance memory usage and CPU utilization. This allows us to maximize the efficiency of the parallel processing while avoiding memory errors (Buddelmeijer et al. 2011; Riccio et al. 2017).

2.8.4. *Timing and Profiling*

We profile the runtime of a single catalog's analysis to ensure that the full set can be completed within the allocated time (Regier et al. 2018). We adjust the batch size or parallelization strategy as needed to optimize the performance (Regier et al. 2018).

3. RESULTS

3.1. *Dependence on Feedback and Cosmological Parameters*

3.1.1. *Multivariate Regression and Feature Importance*

We performed a multivariate linear regression and random forest analysis to determine the dependence of the $M_{\rm BH}$–$M_{\rm star}$ relation on feedback and cosmological parameters. We examined the effects on the slope (β), normalization (α), and scatter of the relation, considering low, intermediate, and high mass bins.

SLOPE (β)

Low Mass Bin: For the slope β in the low mass bin, the most influential parameters are $A_{\rm SN1}$ (SN wind energy per SFR) and $A_{\rm AGN1}$ (AGN feedback energy per accretion). As shown in Figure 1, $A_{\rm SN1}$ exhibits the largest importance, followed by $A_{\rm AGN1}$ in the Random Forest Feature Importance analysis. The standardized coefficient for $A_{\rm SN1}$ is +0.05 with a Random Forest (RF) importance of 0.41, while for $A_{\rm AGN1}$ it is +0.04 with an RF importance of 0.29. Both positively correlate with the slope, indicating that stronger feedback steepens the relation at low mass. Cosmological parameters have weaker effects. This is further illustrated in the partial dependence plots in Figure 2, which show the effect of these parameters on the slope β. The distribution of the slope β for the low mass bin is shown in Figure 3, with a peak around $\beta \approx 0.17$.

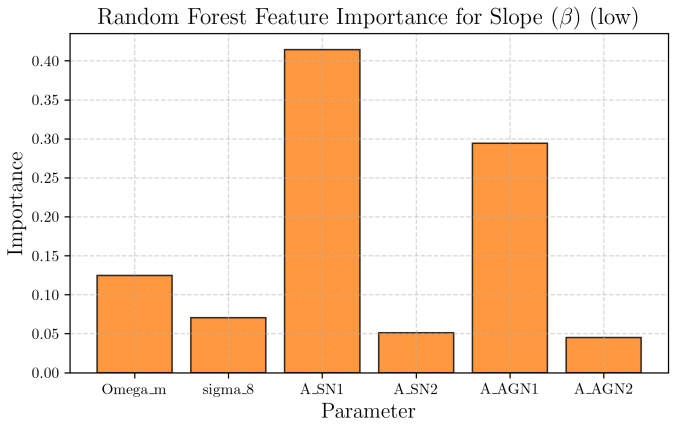

Figure 1. The Random Forest Feature Importance for the slope (β) in the low-redshift regime is shown. The A_SN1 parameter exhibits the largest importance, followed by A_AGN1. The parameters sigma_8, A_SN2, and A_AGN2 show relatively low importance.

Intermediate/High Mass Bins: In contrast, for intermediate and high mass bins, $A_{\rm AGN1}$ becomes the dominant parameter. Figure 6 shows the feature importance for the intermediate mass bin, where $A_{\rm AGN1}$ has the highest importance. The standardized coefficient for $A_{\rm AGN1}$ is +0.37 with an RF importance of 0.88 in the intermediate mass bin, and −0.22 with an RF importance of 0.69 in the high mass bin. This suggests a transition from AGN-driven black hole growth at intermediate mass to AGN-driven suppression at high mass.

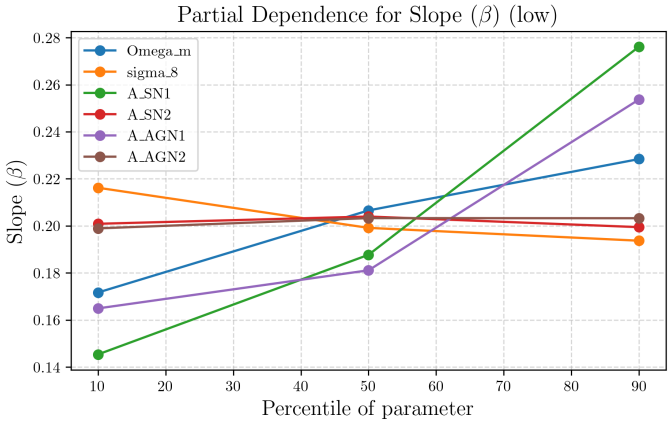

Figure 2. Partial dependence plots for the slope β show the effect of several parameters on the slope. The parameters are Ω_m, σ_8, A_SN1, A_SN2, A_AGN1, and A_AGN2. The x-axis represents the percentile of each parameter, while the y-axis shows the corresponding slope β value. Significant differences are observed in the partial dependence of the slope on the parameters, particularly for A_SN1, A_AGN1, and Ω_m.

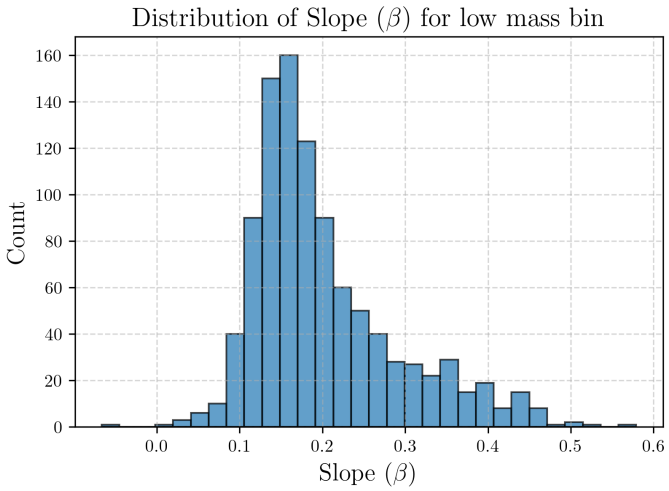

Figure 3. The distribution of the slope, β, for a low mass bin is shown. The histogram indicates a peak around $\beta \approx 0.17$, with a long tail extending to higher values.

Figure 7 shows the partial dependence plots for the intermediate mass bin. $A_{\rm SN1}$ and cosmological parameters have smaller or inconsistent effects. Figure 5 and 4 illustrate the feature importance and partial dependence plots, respectively, for the high mass bin.

NORMALIZATION (α)

Low Mass Bin: For the normalization α in the low mass bin, $A_{\rm SN1}$ and $A_{\rm AGN1}$ have strong negative coefficients (-0.38 and -0.32), indicating that stronger feedback lowers the normalization, i.e., black holes are less

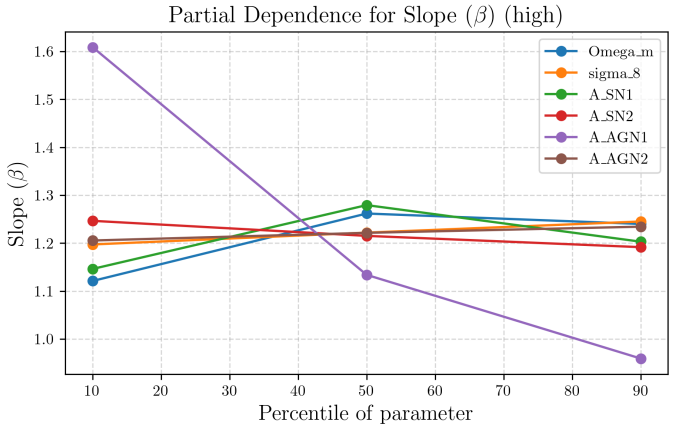

Figure 4. The partial dependence of the slope β on different cosmological parameters. The parameters considered are Ω_m, σ_8, A_{SN1}, A_{SN2}, A_{AGN1}, and A_{AGN2}. The figure shows the variation of the slope β as a function of the percentile of each parameter. Large differences are seen in the dependence of the slope on the A_{AGN1} parameter, while the other parameters show relatively smaller variations.

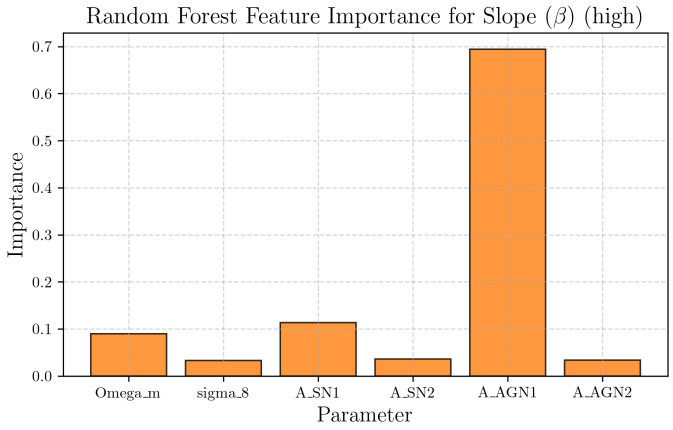

Figure 5. Random Forest Feature Importance for Slope (β) (high). The figure shows the relative importance of different parameters in a Random Forest model predicting the slope (β). A significant difference is observed, with A_AGN1 showing a substantially higher importance compared to other parameters.

massive at fixed stellar mass. This is also reflected in the Random Forest feature importance, shown in Figure 9 and the standardized linear feature importance in Figure 10, where $A_{\rm SN1}$ and $A_{\rm AGN1}$ exhibit the largest importance values compared to the other parameters. Figure 11 shows the partial dependence of the normalization on these parameters. Ω_m also has a negative effect. The distribution of the normalization factor α for the low mass bin is shown in Figure 12, which is skewed towards higher values of α, with a peak around $\alpha \approx 4.7$.

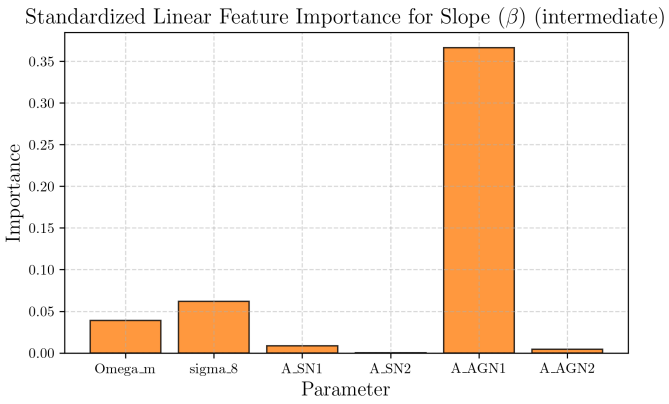

Figure 6. The figure shows the standardized linear feature importance for the slope β parameter, in the intermediate case. The importance is shown for different cosmological parameters and nuisance parameters, namely Ω_m, σ_8, A_{SN1}, A_{SN2}, A_{AGN1}, and A_{AGN2}. A large difference in importance is observed, with A_{AGN1} having the highest importance, significantly larger than the other parameters.

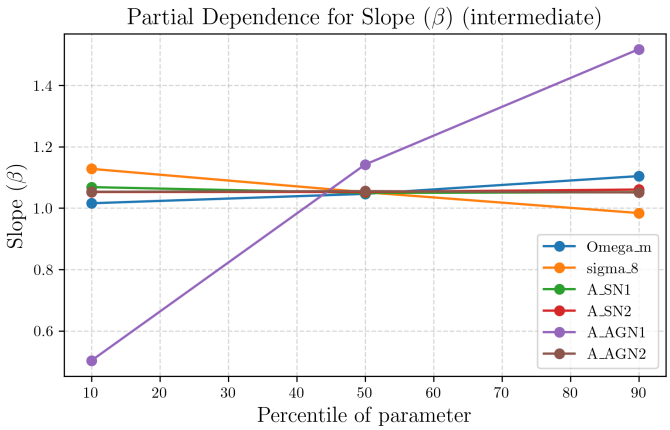

Figure 7. Partial dependence plots for the slope β as a function of the percentile of different parameters. The parameters include cosmological parameters such as Ω_m and σ_8, as well as astrophysical parameters related to supernovae (A_SN1, A_SN2) and active galactic nuclei (A_AGN1, A_AGN2). The A_AGN1 parameter exhibits a large dependence on the percentile, while the other parameters show relatively small changes in the slope β across the percentile range.

Intermediate/High Mass Bins: Again, $A_{\rm AGN1}$ is the dominant driver for intermediate and high mass bins, as illustrated by Figures 14, 15, and 13. The standardized coefficients are -3.32 and $+2.52$ for intermediate and high mass bins respectively, with the sign flip again reflecting a regime change. The partial dependence plots in Figures 16 and 17 show the variation of α with respect to the percentile of different parameters. σ_8 and Ω_m also contribute, with higher matter density

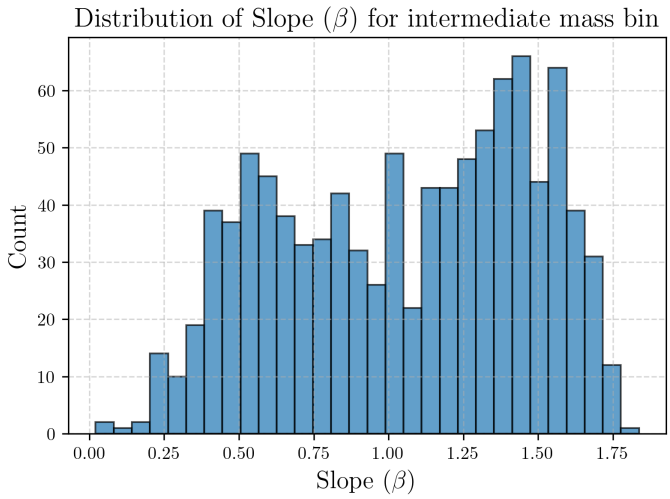

Figure 8. The figure shows the distribution of the slope β parameter for an intermediate mass bin. The distribution displays a range of slopes, with a concentration of values around 0.5-0.6 and between 1.4-1.6.

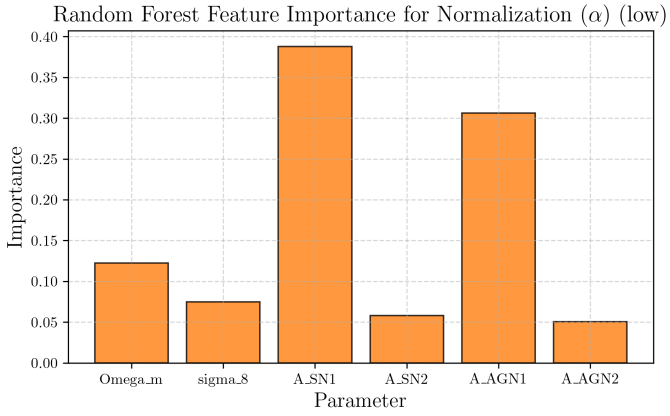

Figure 9. Random Forest Feature Importance for Normalization with a low normalization parameter α. The bar plot illustrates the importance of different cosmological parameters (Omega_m, sigma_8, A_SN1, A_SN2, A_AGN1, A_AGN2) as determined by the Random Forest algorithm. Large differences in feature importance are observed, with A_SN1 and A_AGN1 showing the highest importance, while sigma_8 and A_SN2 exhibit relatively lower importance.

and power spectrum normalization generally lowering α. The distribution of α for the intermediate mass bin is shown in Figure 18, which displays a multi-modal distribution.

SCATTER

Low Mass Bin: For the scatter in the low mass bin, $A_{\rm SN1}$ is the primary driver of increased scatter, with a coefficient of $+0.04$ and an RF importance of 0.73. This is consistent with the expectation that stochastic SN

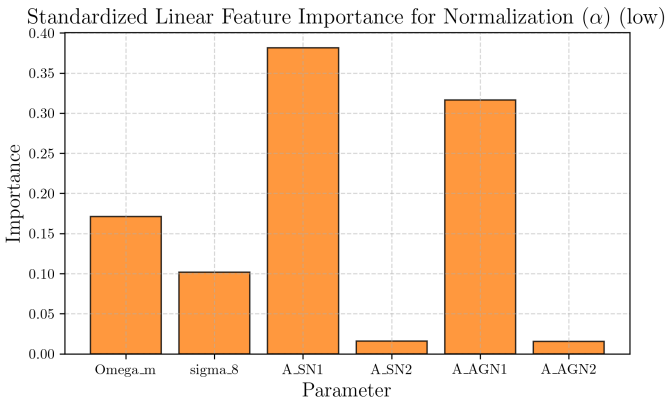

Figure 10. The figure displays the standardized linear feature importance for normalization with a low alpha value. The importance is shown for cosmological parameters Omega_m and sigma_8, as well as parameters related to Supernovae (SN1, SN2) and Active Galactic Nuclei (AGN1, AGN2). A_SN1 and A_AGN1 exhibit the largest importance values compared to the other parameters.

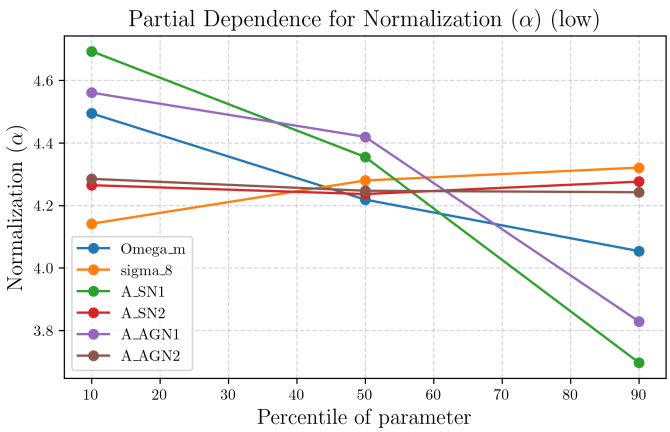

Figure 11. The figure shows the partial dependence for the normalization α at low values, as a function of the percentile of different parameters. The parameters considered are Omega_m, sigma_8, A_SN1, A_SN2, A_AGN1, and A_AGN2. Large differences are observed in the normalization α for different parameters, with A_SN1 and A_AGN1 showing the most significant decrease as the percentile of the parameter increases. Omega_m also shows a decreasing trend, while sigma_8, A_SN2, and A_AGN2 show relatively small changes with percentile.

feedback introduces diversity in black hole growth histories. The feature importance plots in Figures 19 and 20 highlight the dominance of $A_{\rm SN1}$. The partial dependence plot in Figure 21 further illustrates this. The distribution of scatter values for the low mass bin is shown in Figure 22.

Intermediate/High Mass Bins: For intermediate and high mass bins, $A_{\rm AGN1}$ and $A_{\rm SN1}$ both contribute.

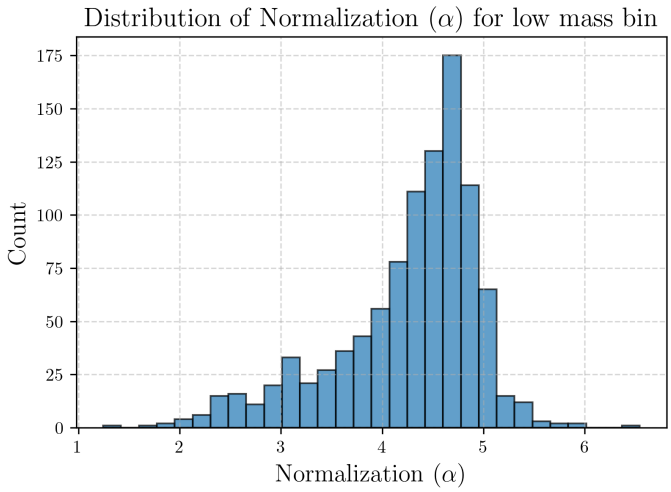

Figure 12. The figure displays the distribution of the normalization factor α for a low mass bin. The histogram reveals a distribution that is skewed towards higher values of α, with a peak around $\alpha \approx 4.7$.

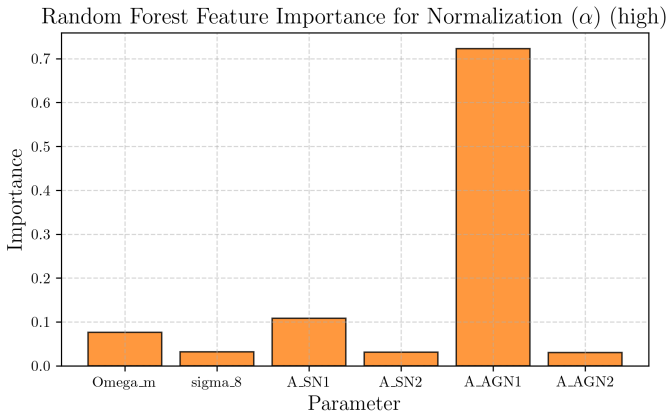

Figure 13. Random Forest feature importance for Normalization (α) with high α values. The plot shows the relative importance of different cosmological parameters (Omega_m, sigma_8, A_SN1, A_SN2, A_AGN1, A_AGN2) as determined by a Random Forest model. A_AGN1 exhibits a significantly higher importance compared to the other parameters, indicating its dominant role in the normalization process when α is high.

$A_{\rm AGN1}$ increases scatter at intermediate mass (RF 0.44) and $A_{\rm SN1}$ at high mass (RF 0.31). The distribution of scatter for the intermediate mass bin is shown in Figure 23. Figure 24 shows the feature importance for the high scatter scenario, where $A_{\rm AGN1}$ is the most important parameter, followed by $A_{\rm SN1}$.

3.2. *Cosmological Parameters*

Ω_m and σ_8 have secondary but non-negligible effects, especially on normalization and scatter. Higher Ω_m gen-

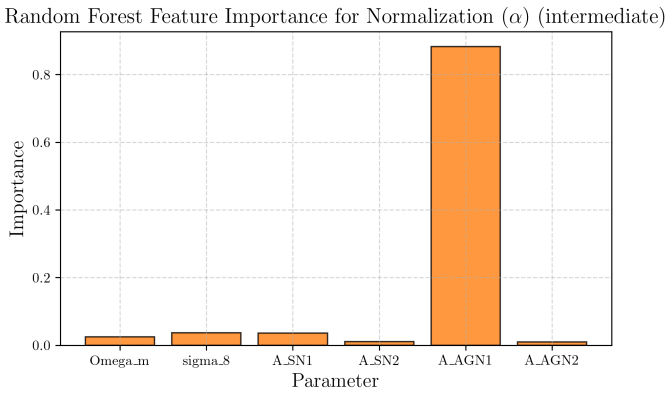

Figure 14. Random Forest Feature Importance for Normalization (α) (intermediate) indicates that the parameter 'A_AGN1' is significantly more important than the other parameters ('Omega_m', 'sigma_8', 'A_SN1', 'A_SN2', 'A_AGN2') for normalization. The importance of 'A_AGN1' is approximately 0.9, while the importance of the other parameters is close to 0.

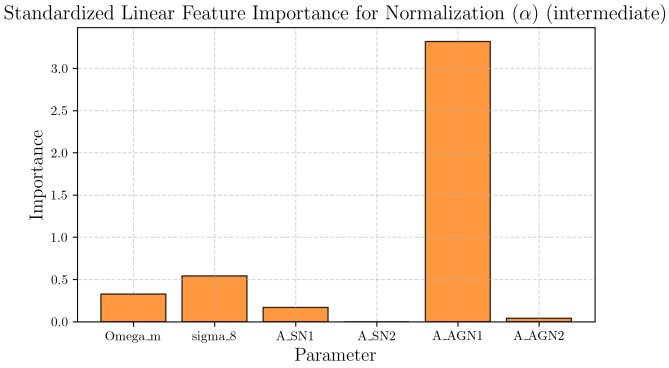

Figure 15. Standardized linear feature importance for normalization (α) in the intermediate case. The parameter A_AGN1 has a significantly larger importance compared to the other parameters, indicating it is the most influential factor in the normalization process.

erally lowers normalization and increases scatter, while higher σ_8 can either increase or decrease normalization depending on mass bin.

3.3. *Black Hole Occupation Fraction*

The occupation fraction rises from ∼0.72 at low mass to ∼0.96 at high mass. Stronger SN feedback ($A_{\rm SN1}$) reduces the occupation fraction at low and intermediate mass, consistent with the suppression of black hole formation or growth in shallow potential wells. AGN feedback has a weaker effect on occupation at low mass but becomes more important at high mass. The incomplete occupation at low mass, and its sensitivity to feedback, supports models in which black hole seeding is inefficient

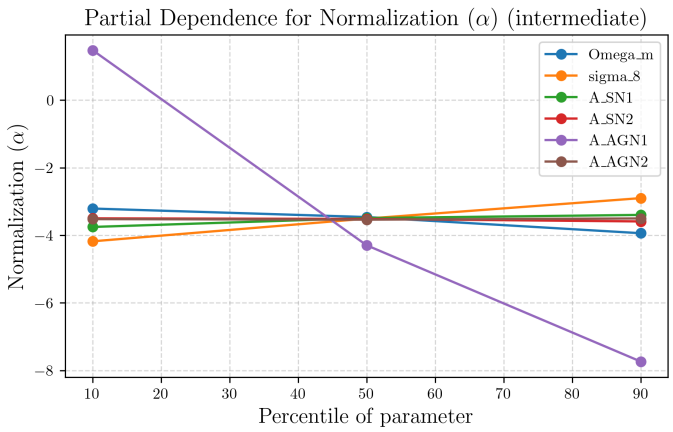

Figure 16. Partial dependence plot for the normalization parameter α as a function of the percentile of different cosmological parameters and survey characteristics. A large dependence on the percentile of A_AGN1 parameter is seen, while the other parameters show a small dependence.

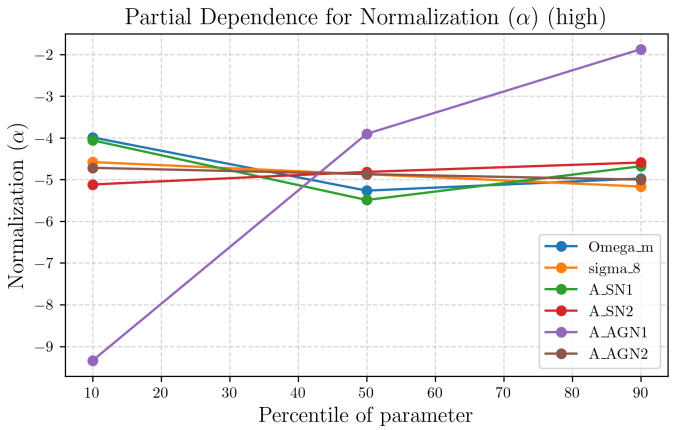

Figure 17. Partial dependence plot for the normalization factor α at high values. The plot shows the variation of α with respect to the percentile of different parameters: Ω_m, σ_8, A_{SN1}, A_{SN2}, A_{AGN1}, and A_{AGN2}. While Ω_m, σ_8, A_{SN1}, A_{SN2}, and A_{AGN2} exhibit relatively small changes in α across the parameter percentile range, A_{AGN1} shows a more significant increase in α as the parameter percentile increases.

or stochastic in low-mass halos, and can be suppressed by energetic feedback.

3.4. *Synthesis and Physical Interpretation*

The results demonstrate that the diversity in the $M_{\rm BH}$–$M_{\rm star}$ relation is primarily driven by the strength and mode of feedback, with SN feedback dominating at low mass and AGN feedback at high mass. The transition between these regimes is marked by a shift in the sign and magnitude of the feedback coefficients, and is accompanied by changes in the occupation fraction and

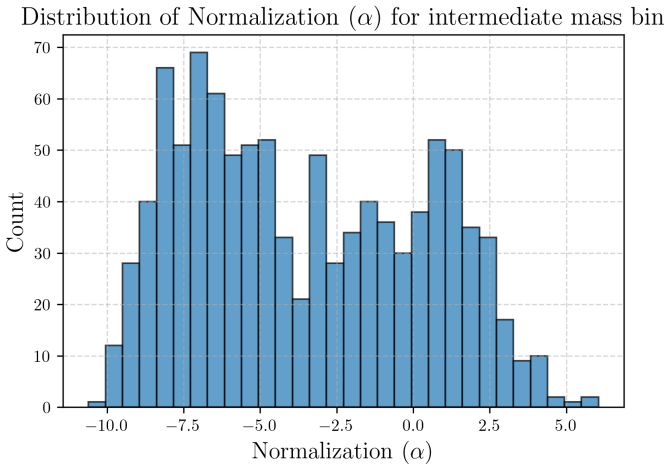

Figure 18. The figure shows the distribution of the normalization parameter α for an intermediate mass bin. The distribution is multi-modal, with peaks around -7, -5, -2, and 1. This suggests that there are significant variations in the normalization values within this mass range.

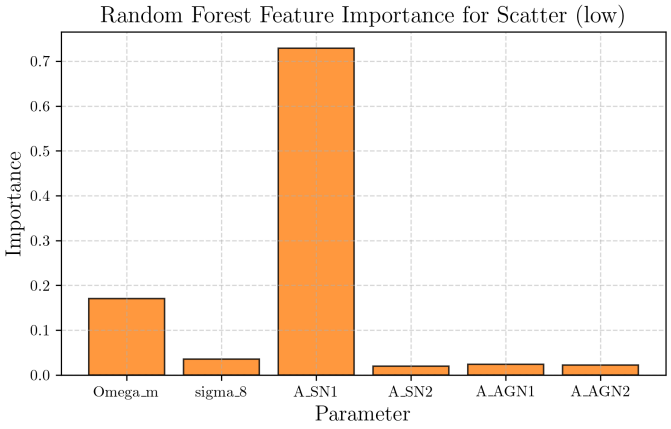

Figure 20. Random Forest Feature Importance for Scatter (low) shows the relative importance of different parameters when scatter is low. A_SN1 is the most important parameter. Omega_m is also important. The remaining parameters have low importance.

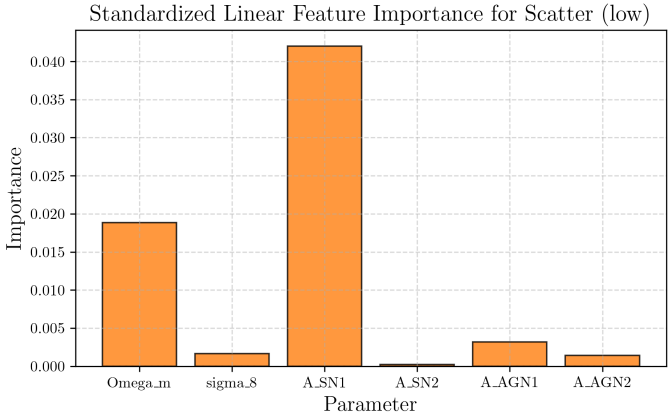

Figure 19. Standardized linear feature importance for scatter (low). The plot shows the relative importance of different cosmological parameters on the scatter. A_SN1 exhibits the largest importance, followed by Omega_m, while the other parameters have relatively small importance.

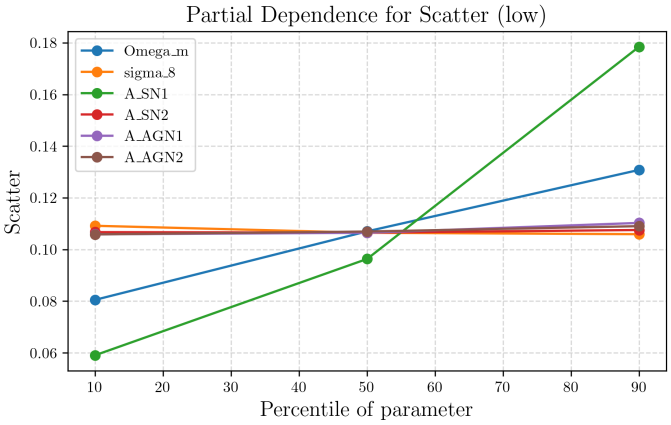

Figure 21. Partial dependence plot for the scatter, showing the impact of different parameters on the scatter. The x-axis represents the percentile of each parameter, and the y-axis represents the scatter. Large differences are seen in the scatter as a function of the percentile of parameter.

scatter. While feedback is the dominant driver, cosmological parameters modulate the normalization and scatter, particularly in the intermediate and high mass bins. The broad range of slopes, normalizations, and scatters observed across the simulated catalogs underscores the potential for significant diversity in the $M_{\rm BH}$–$M_{\rm star}$ relation in the real universe, especially in regimes where feedback is strong or stochastic. The sensitivity of the occupation fraction to feedback at low mass provides a direct link between black hole seeding models and the observable demographics of low-mass galaxies.

4. CONCLUSIONS

In this work, we presented a comprehensive analysis of the black hole–stellar mass ($M_{\rm BH}$–$M_{\rm star}$) relation, leveraging a suite of 1,000 cosmological hydrodynamic simulations spanning a wide range of cosmological and feedback parameter space. The primary goal was to systematically quantify how the slope, normalization, and scatter of this fundamental scaling relation vary as a function of key cosmological parameters (Ω_m, σ_8) and feedback parameters (A_{SN1}, A_{SN2}, A_{AGN1}, A_{AGN2}). By exploring this unprecedented parameter space, we aimed to reveal the physical drivers of scaling relation diversity and identify potential secondary dependencies in galaxy evolution.

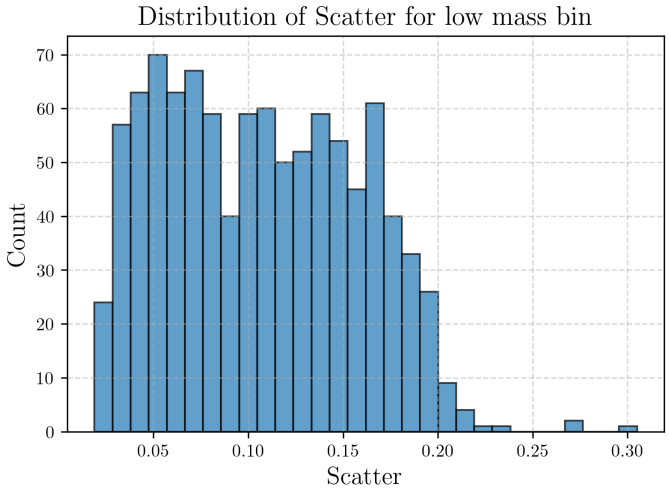

Figure 22. Distribution of Scatter for low mass bin. The histogram shows the distribution of the scatter for a low mass bin. The scatter values range from approximately 0.025 to 0.3, with a peak between 0.05 and 0.075. The distribution is skewed to the right, with a long tail extending towards higher scatter values.

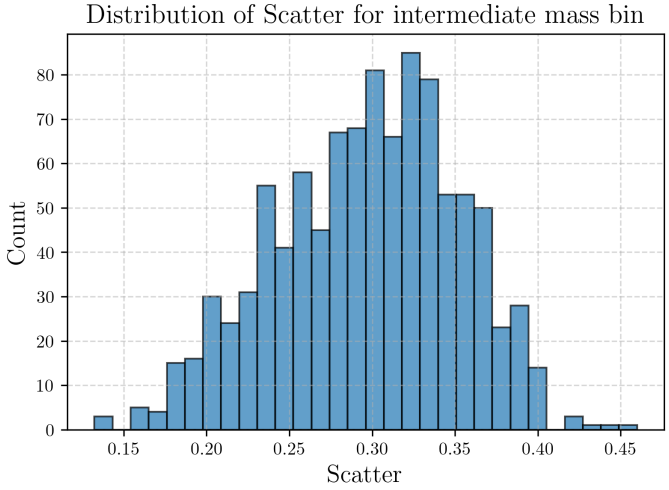

Figure 23. Distribution of the scatter values for an intermediate mass bin. The distribution peaks around a scatter value of 0.32, indicating a concentration of data points within this range.

Our analysis involved fitting the $M_{\rm BH}$–$M_{\rm star}$ relation in three distinct stellar mass bins, excluding galaxies with $M_{\rm BH} = 0$ to focus on galaxies hosting detectable black holes. We then performed a multivariate regression analysis, employing both linear and random forest techniques, to map the dependence of the relation's parameters (slope, normalization, and scatter) on the cosmological and feedback parameters. Additionally, we quantified the black hole occupation fraction as a function of stellar mass and feedback, providing insights into the prevalence of black holes in different galaxy populations.

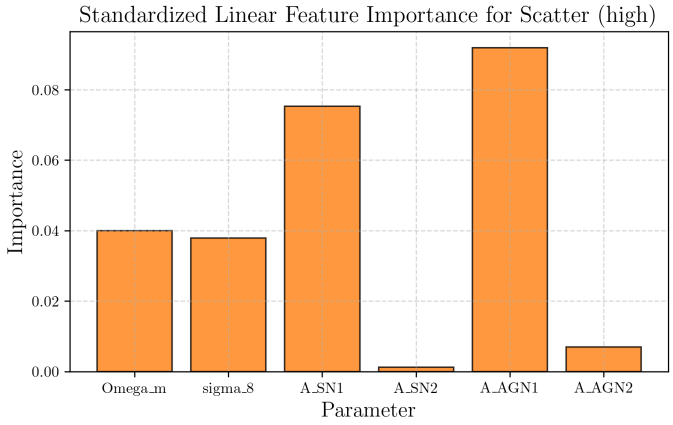

Figure 24. Standardized linear feature importance for a high scatter scenario. The plot shows the relative importance of different cosmological parameters (Omega_m, sigma_8, A_SN1, A_SN2, A_AGN1, A_AGN2) in influencing the scatter. Large differences in importance are observed, with A_AGN1 being the most important parameter, followed by A_SN1. A_SN2 and A_AGN2 show very low importance.

The results reveal a significant diversity in the $M_{\rm BH}$–$M_{\rm star}$ relation across the simulated catalogs. We found that the slope and normalization of the relation vary substantially, particularly in the intermediate and high mass bins, highlighting the sensitivity of black hole-galaxy coevolution to the underlying physical parameters. The scatter of the relation increases with stellar mass, suggesting that stochastic processes become more important in more massive galaxies. Furthermore, the black hole occupation fraction rises with stellar mass, indicating that black holes are more common in larger galaxies.

Our analysis demonstrates that feedback processes, particularly supernova (SN) and active galactic nuclei (AGN) feedback, are the primary drivers of the observed diversity in the $M_{\rm BH}$–$M_{\rm star}$ relation. At low stellar masses, SN feedback plays a dominant role, influencing the slope, normalization, and scatter of the relation, as well as the black hole occupation fraction. At higher stellar masses, AGN feedback becomes increasingly important, affecting the relation in a complex manner that depends on the specific mass regime. While cosmological parameters have a secondary influence, they modulate the normalization and scatter of the relation, highlighting the interplay between cosmological and baryonic processes in shaping galaxy evolution.

The findings presented in this paper provide valuable insights into the coevolution of black holes and galaxies.

By systematically mapping the diversity of the $M_{\rm BH}$–$M_{\rm star}$ relation across a wide range of parameter space, we have identified the key physical drivers of this fundamental scaling relation. These results underscore the importance of feedback processes in regulating black hole growth and shaping the properties of galaxies. Furthermore, our analysis of the black hole occupation fraction provides constraints on black hole seeding models and sheds light on the prevalence of black holes in different galaxy populations. This work contributes to a deeper understanding of the complex interplay between black holes and their host galaxies and lays the foundation for future studies incorporating additional observables and exploring the evolution of these relations across cosmic time.

REFERENCES

Akritas, M. G., & Siebert, J. 1995, A test for partial correlation with censored astronomical data, doi: https://doi.org/10.1093/mnras/278.4.919

Baker, W. M., Maiolino, R., Bluck, A. F. L., et al. 2024, Different regulation of stellar metallicities between star-forming and quiescent galaxies – Insights into galaxy quenching. https://arxiv.org/abs/2309.00670

Bhowmick, A. K., Blecha, L., Torrey, P., et al. 2023, Representing low mass black hole seeds in cosmological simulations: A new sub-grid stochastic seed model. https://arxiv.org/abs/2309.15341

Buddelmeijer, H., Boxhoorn, D., & Valentijn, E. A. 2011, Automatic Optimized Discovery, Creation and Processing of Astronomical Catalogs. https://arxiv.org/abs/1111.3784

Burke, C. J., Natarajan, P., Baldassare, V. F., & Geha, M. 2025, Multi-wavelength constraints on the local black hole occupation fraction. https://arxiv.org/abs/2410.11177

Capelo, P. R., Feruglio, C., Hickox, R. C., & Tombesi, F. 2022, Black hole-galaxy co-evolution and the role of feedback, doi: https://doi.org/10.1007/978-981-16-4544-0_115-1

Chen, Y., Gu, Q., Fan, J., et al. 2025, The relation between black hole spin, star formation rate, and black hole mass for supermassive black holes. https://arxiv.org/abs/2503.03223

Cohn, J. H., Durodola, E., Casey, Q. O., Lambrides, E., & Hickox, R. C. 2025, Evidence for evolutionary pathway-dependent black hole scaling relations. https://arxiv.org/abs/2504.00172

Crain, R. A., & van de Voort, F. 2023, Hydrodynamical simulations of the galaxy population: enduring successes and outstanding challenges, doi: https://doi.org/10.1146/annurev-astro-041923-043618

Cui, C., Fan, D., Zhao, Y., et al. 2011, Enhanced Management of Personal Astronomical Data with FITSManager, doi: https://doi.org/10.1016/j.newast.2011.06.009

Davis, B. L., Graham, A. W., & Cameron, E. 2019, Black Hole Mass Scaling Relations for Spiral Galaxies. II. $M_{\rm BH}$-$M_{*,\rm tot}$ and $M_{\rm BH}$-$M_{*,\rm disk}$, doi: https://doi.org/10.3847/1538-4357/aae820

de Santi, N. S. M., Villaescusa-Navarro, F., Abramo, L. R., et al. 2025, Field-level simulation-based inference with galaxy catalogs: the impact of systematic effects, doi: https://doi.org/10.1088/1475-7516/2025/01/082

Ding, J., Li, S., Zheng, Y., et al. 2023, Fast generation of mock galaxy catalogues with COLA, doi: https://doi.org/10.3847/1538-4365/ad0c5b

Ding, X., Silverman, J., Treu, T., et al. 2019, The mass relations between supermassive black holes and their host galaxies at 1<z<2 with HST-WFC3, doi: https://doi.org/10.3847/1538-4357/ab5b90

Dou, J., Peng, Y., Gu, Q., et al. 2025, The critical role of dark matter halos in driving star formation. https://arxiv.org/abs/2503.04243

Farahi, A., Anbajagane, D., & Evrard, A. 2022, KLLR: A scale-dependent, multivariate model class for regression analysis, doi: https://doi.org/10.3847/1538-4357/ac6ac7

Gallo, E., Hodges-Kluck, E., Treu, T., et al. 2019, Towards a high accuracy measurement of the local black hole occupation fraction in low mass galaxies. https://arxiv.org/abs/1903.06629

—. 2023, The black hole occupation fraction of local dwarf galaxies with AXIS. https://arxiv.org/abs/2311.09161

Georgakakis, A., Papadakis, I., & Paolillo, M. 2021, Exploring black-hole scaling relations via the ensemble variability of Active Galactic Nuclei, doi: https://doi.org/10.1093/mnras/stab2818

Group, T. D. H. D. S., Balázs, C., van Beekveld, M., et al. 2021, A comparison of optimisation algorithms for high-dimensional particle and astrophysics applications, doi: https://doi.org/10.1007/JHEP05(2021)108

Gómez, J. S., Yepes, G., Muñoz, A. J., & Cui, W. 2024, Galaxy catalogs from the SAGE Semi-Analytic Model calibrated on THE THREE HUNDRED hydrodynamical simulations: A method to push the limits toward lower mass galaxies in dark matter only clusters simulations, doi: https://doi.org/10.1051/epjconf/202429300023

Hoffman, K., Sung, J. Y., & Zazzera, A. 2021, Multi-Output Random Forest Regression to Emulate the Earliest Stages of Planet Formation. https://arxiv.org/abs/2104.12845

Jin, Z., & Davis, B. L. 2023, Discovering Black Hole Mass Scaling Relations with Symbolic Regression. https://arxiv.org/abs/2310.19406

Jin, Z., Pasquato, M., Davis, B. L., et al. 2025, Causal Discovery in Astrophysics: Unraveling Supermassive Black Hole and Galaxy Coevolution, doi: https://doi.org/10.3847/1538-4357/ad9ded

Jung, M., Roca-Fàbrega, S., hoon Kim, J., et al. 2024, The AGORA High-resolution Galaxy Simulations Comparison Project. V: Satellite Galaxy Populations In A Cosmological Zoom-in Simulation of A Milky Way-mass Halo, doi: https://doi.org/10.3847/1538-4357/ad245b

Juodžbalis, I., Maiolino, R., Baker, W. M., et al. 2024, A dormant, overmassive black hole in the early Universe, doi: https://doi.org/10.1038/s41586-024-08210-5

Kent, B. R. 2017, Editorial: Techniques and Methods for Astrophysical Data Visualization, doi: https://doi.org/10.1088/1538-3873/aa5fa6

Kumar, A., Ayyalasomayajula, M. M. T., Panwar, D., & Vasa, Y. 2024, Optimizing Photometric Light Curve Analysis: Evaluating Scipy's Minimize Function for Eclipse Mapping of Cataclysmic Variables, doi: https://doi.org/10.52783/jes.4079

Lamastra, A., Menci, N., Maiolino, R., Fiore, F., & Merloni, A. 2010, The Building Up of the Black Hole Mass - Stellar Mass Relation, doi: https://doi.org/10.1111/j.1365-2966.2010.16439.x

Lan, F., Young, M., Anderson, L., et al. 2021, Visualization in Astrophysics: Developing New Methods, Discovering Our Universe, and Educating the Earth. https://arxiv.org/abs/2106.00152

Lehman, K., Krippendorf, S., Weller, J., & Dolag, K. 2024, Learning Optimal and Interpretable Summary Statistics of Galaxy Catalogs with SBI. https://arxiv.org/abs/2411.08957

Li, X., Li, C., & Mo, H. 2024, What drives the HI content of central galaxies – A comparison between hydrodynamic simulations and observations using Random Forest. https://arxiv.org/abs/2411.07977

Lin, Y.-T., Chen, K.-F., Chen, T.-C., Chuang, C.-Y., & Oguri, M. 2025, Evolution of Massive Red Galaxies in Clusters from z=1.0 to z=0.3. https://arxiv.org/abs/2503.13592

Martin-Navarro, I., & Mezcua, M. 2018, Exploring the limits of AGN feedback: black holes and the star formation histories of low-mass galaxies, doi: https://doi.org/10.3847/2041-8213/aab103

Merritt, D. 1999, Black Holes and Galaxy Evolution. https://arxiv.org/abs/astro-ph/9910546

Montaguth, G. P., Monachesi, A., Torres-Flores, S., et al. 2025, Galaxy evolution in compact groups II. Witnessing the influence of major structures in their evolution. https://arxiv.org/abs/2406.14671

Narkedimilli, S., Amballa, V. S., Kumar, N. V. S., et al. 2025, Comparative Analysis of Black Hole Mass Estimation in Type-2 AGNs: Classical vs. Quantum Machine Learning and Deep Learning Approaches. https://arxiv.org/abs/2502.15297

Pacifici, C., Kassin, S. A., Weiner, B. J., et al. 2016, The evolution of star formation histories of quiescent galaxies, doi: https://doi.org/10.3847/0004-637X/832/1/79

Pacucci, F., & Loeb, A. 2024, The Redshift Evolution of the $M_\bullet - M_\star$ Relation for JWST's Supermassive Black Holes at $z > 4$, doi: https://doi.org/10.3847/1538-4357/ad3044

Peirani, S., Suto, Y., Beckmann, R. S., et al. 2024, Cosmic evolution of black hole-spin and galaxy orientations: clues from the NewHorizon and Galactica simulations, doi: https://doi.org/10.1051/0004-6361/202349101

Popesso, P., Marini, I., Dolag, K., et al. 2024, Average X-ray properties of galaxy groups. From Milky Way-like halos to massive clusters. https://arxiv.org/abs/2411.17120

Porras-Valverde, A. J., & Forbes, J. C. 2024, On the signature of black holes on the quenched stellar mass function. https://arxiv.org/abs/2412.04553

Regier, J., Pamnany, K., Fischer, K., et al. 2018, Cataloging the Visible Universe through Bayesian Inference at Petascale. https://arxiv.org/abs/1801.10277

Reines, A. E., & Volonteri, M. 2015, Relations Between Central Black Hole Mass and Total Galaxy Stellar Mass in the Local Universe, doi: https://doi.org/10.1088/0004-637X/813/2/82

Riccio, G., Brescia, M., Cavuoti, S., et al. 2017, C^3 : A Command-line Catalogue Cross-matching tool for modern astrophysical survey data, doi: https://doi.org/10.1017/S1743921316013120

Schawinski, K. 2012, Black Hole – Galaxy Co-evolution. https://arxiv.org/abs/1206.2661

Sereno, M. 2015, A Bayesian approach to linear regression in astronomy. https://arxiv.org/abs/1509.05778

Sturm, M. R., & Reines, A. E. 2024, A Breakdown of the Black Hole - Bulge Mass Relation in Local Active Galaxies. https://arxiv.org/abs/2406.06675

Su, C., Shan, H., Zhao, C., Xu, W., & Zhang, J. 2025, Cosmological Constraints with Void Lensing I: the Simulation-Based Inference Framework. https://arxiv.org/abs/2504.15149

Tan, Z., Yan, J., Hsu, I.-H., et al. 2025, In Prospect and Retrospect: Reflective Memory Management for Long-term Personalized Dialogue Agents. https://arxiv.org/abs/2503.08026

Terrazas, B. A., Bell, E. F., Woo, J., & Henriques, B. M. B. 2017, Supermassive black holes as the regulators of star formation in central galaxies, doi: https://doi.org/10.3847/1538-4357/aa7d07

Tremmel, M., Ricarte, A., Natarajan, P., et al. 2024, An Enhanced Massive Black Hole Occupation Fraction Predicted in Cluster Dwarf Galaxies, doi: https://doi.org/10.33232/001c.116617

Tudisco, G., Vitello, F., Sciacca, E., & Becciani, U. 2025, From Local to Remote: VisIVO Visual Analytics in the Era of the Square Kilometre Array. https://arxiv.org/abs/2503.24113

Wechsler, R. H., DeRose, J., Busha, M. T., et al. 2021, ADDGALS: Simulated Sky Catalogs for Wide Field Galaxy Surveys, doi: https://doi.org/10.3847/1538-4357/ac5b0a

Winkel, N., Bennert, V. N., Remigio, R. P., et al. 2024, Combining Direct Black Hole Mass Measurements and Spatially Resolved Stellar Kinematics to Calibrate the $M_{\rm BH}$-$\sigma_\star$ Relation of Active Galaxies. https://arxiv.org/abs/2411.02488

Yang, G., Chen, C. T. J., Vito, F., et al. 2017, Black-Hole Growth is Mainly Linked to Host-Galaxy Stellar Mass rather than Star Formation Rate, doi: https://doi.org/10.3847/1538-4357/aa7564

Yang, Y., Bird, S., & Ho, M.-F. 2025, Ten-parameter simulation suite for cosmological emulation beyond ΛCDM. https://arxiv.org/abs/2501.06296

Yao, S., Qiao, E., Wu, X.-B., & You, B. 2018, Exploring the physics of the accretion and jet in nearby narrow-line Seyfert 1 galaxies, doi: https://doi.org/10.1093/mnras/sty788

Zavala, J., & Frenk, C. S. 2019, Dark matter haloes and subhaloes. https://arxiv.org/abs/1907.11775

Zhang, Y., Ouchi, M., Gebhardt, K., et al. 2023, The Stellar Mass - Black Hole Mass Relation at $z \sim 2$ Down to $\mathcal{M}_{\rm BH} \sim 10^7 M_\odot$ Determined by HETDEX, doi: https://doi.org/10.3847/1538-4357/acc2c2

Zhu, P., Ho, L. C., & Gao, H. 2020, The Correlation between Black Hole Mass and Stellar Mass for Classical Bulges and the Cores of Ellipticals, doi: https://doi.org/10.3847/1538-4357/abcaa1